Composites in Construction 2005 – Third International Conference, Hamelin et al (eds) © 2005 ISBN xxxxx

Lyon, France, July 11 – 13, 2005

FRACTURE MECHANICAL BEHAVIOR OF E-GLASS/POLYESTER COMPOSITE SYSTEMS UNDER MODE-II AND MIXED-MODE I/II LOADING

A. Szekrényes and J. Uj,
Department of Applied Mechanics, Budapest University of Technology and Economics
Budapest, P.O.Box 11, H-1521, Hungary
szeki@mm.bme.hu uj@mm.bme.hu

ABSTRACT: In the current research we present a combined experimental and analytical investigation for two novel interlaminar fracture specimens: the mode-II over-notched flexure (ONF) and the mixed-mode I/II over-leg bending (OLB) specimens. In the first part of the work we introduce the analytical compliance and strain energy release rate expressions, while in the second part of our presentation we demonstrate the details of the experimental systems together with the experimental results. Comparison between the analytical and experimental results is included and a very good agreement may be established in both specimens. Apart from that, the presented ONF and OLB specimens show similar fracture mechanical behavior, which is also highlighted in the presentation.

1. INTRODUCTION

The interlaminar fracture in composite materials is characterized by using different types of specimens, which can be treated as slender beams. To obtain a complete interlaminar fracture envelope for the material the critical strain energy release rate (G_C) needs to be determined under mode-I (G_I), mode-II (G_{II}) and the mixed-mode I/II ($G_{I/II}$) loading. While for mode-I delamination the double-cantilever beam (DCB) specimen [1] is a well-understood tool, for mode-II and mixed-mode I/II cases there are many configurations, which have advantages and relative drawbacks.

For mode-II testing six specimens are available. The end-notched flexure (ENF) specimen is the subject in most of the investigation [2]. Later, the stabilized form of the ENF specimen (SENF) [3] was proposed. The end-loaded split (ELS) [4], the four-point bend ENF (4ENF) [5] and the over-notched flexure (ONF) specimens [6] are also popular mode-II configurations. Finally, the tapered ENF (TENF) specimen [7] should be mentioned as an efficient mode-II geometry.

Numerous mixed-mode I/II configurations are available in the literature, and the development of these setups is still progress in nowadays. The most universal one is the mixed-mode bending (MMB) [8], since it allows to determine a complete fracture envelope. However, to the best of our knowledge only in the case of crack initiation. The single-leg bending (SLB) [9] and the single-

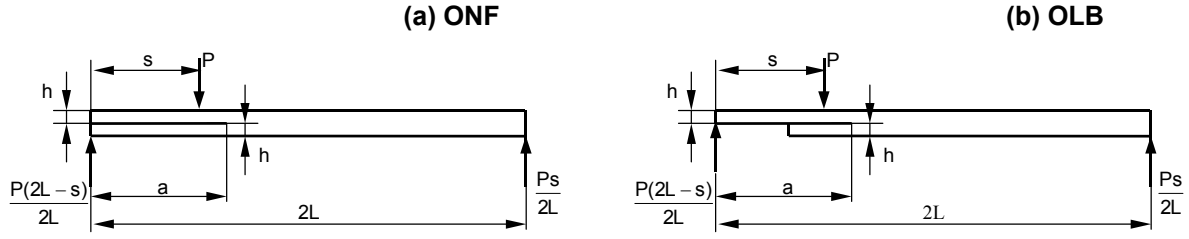

Figure 1 – The mode-II ONF (a) and the mixed-mode I/II OLB (b) delamination specimens.

cantilever beam (SCB) [10] are also the subjects of studies on interlaminar fracture.

In the present work the mode-II and mixed-mode I/II delamination in E-glass/polyester composite is investigated by using the ONF (Figure 1a) and the novel over-leg bending (OLB, Figure 1b) specimens [11], respectively. A beam theory based delamination model [12] is applied to derive the compliance and the strain energy release rate (SERR) of the specimens. Furthermore, experiments on unidirectional specimens are performed and the experimental data is evaluated by means of the compliance calibration and the analytical method. Finally, there is some discussion on the obtained results.

2. DELAMINATION MODEL – BEAM THEORY

In our last work the following equations were presented for the mode-I and mode-II energy release rate of beam-like fracture specimens [12]:

$$G_I = \frac{M_I^2(12 + f_{WP2} + f_{SV2} + f_{T2})}{b^2 h^3 E_{11}}, \qquad G_{II} = \frac{M_{II}^2(9 + f_{SH2})}{b^2 h^3 E_{11}}, \tag{1}$$

where the mode-I and mode-II bending moments are:

$$M_I = (M_1 - M_2)/2, \qquad M_{II} = (M_1 + M_2)/2, \tag{2}$$

where M_1 and M_2 are reduced bending moments at the crack tip. The functions in Eqs. 1 and 2 are [12]:

$$f_{WP2} = 10.14\left(\frac{h}{a}\right)\left(\frac{E_{11}}{E_{33}}\right)^{\frac{1}{4}} + 8.58\left(\frac{h}{a}\right)^2\left(\frac{E_{11}}{E_{33}}\right)^{\frac{1}{2}}, \qquad f_{SV2} = \frac{12}{\pi}\left(\frac{h}{a}\right)\left(\frac{E_{11}}{G_{13}}\right)^{\frac{1}{2}} \tag{3}$$

$$f_{T2} = \frac{1}{k}\left(\frac{h}{a}\right)^2\left(\frac{E_{11}}{G_{13}}\right), \qquad f_{SH2} = 1.96\left(\frac{h}{a}\right)\left(\frac{E_{11}}{G_{13}}\right)^{\frac{1}{2}} + 0.43\left(\frac{h}{a}\right)^2\left(\frac{E_{11}}{G_{13}}\right), \tag{4}$$

where the first in Eq. 3 incorporates the effect of Winkler-Pasternak foundation, the second in Eq. 3 takes the Saint Venant effect into account, while the first in Eq. 4 accounts for transverse shear effect and the second in Eq. 4 considers shear deformation of the crack tip [13]. Furthermore, ‘b’ is the specimen width, ‘h’ is thickness, ‘E_{11}‘ is the flexural modulus, ‘E_{33}‘ is the transverse elastic modulus, ‘G_{13}‘ is the shear modulus, k=5/6 is the shear correction factor and ‘a’ is the crack length.

The derivation of the compliance of the ONF specimen is slightly complicated, a beam theory-based approach resulted in the following compliance expression for the ONF specimen [14]:

$$\begin{aligned} C^{ONF} = {} & \frac{s^2c^3}{8bh^3E_{11}L^2}\left[1 + 4\frac{a}{c} + 8\frac{aL}{c^2} + 16\frac{aL^2}{c^3} + 8\frac{Ls(s-4L)}{c^3}\right] + \frac{s(2L-s)}{4bhkG_{13}L} + \\ & + \frac{s^2c^3}{8bh^3E_{11}L^2}\left[0.98\left(\frac{h}{c}\right)\left(\frac{E_{11}}{G_{13}}\right)^{\frac{1}{2}} + 0.43\left(\frac{h}{c}\right)^2\left(\frac{E_{11}}{G_{13}}\right)\right], \end{aligned} \tag{5}$$

where ‘c’ is the length of the uncracked region (2L-a), ‘s’ is the position of the applied load and ‘L’ is half of the span length (refer to Figure 1). The first term is from Euler-Bernoulli beam theory, the

second one is from Timoshenko beam theory and the last term from crack tip deformation analysis. For the ONF specimen the reduced bending moments at the crack tip are: $M_1=M_2=P(2L-s)/4L$, the application of Eq. 1 results only in a mode-II component:

$$G_{II}^{ONF} = \frac{9P^2s^2c^2}{16b^2h^3E_{11}L^2}\left[1+0.22\left(\frac{h}{c}\right)\left(\frac{E_{11}}{G_{13}}\right)^{\frac{1}{2}}+0.048\left(\frac{h}{c}\right)^2\left(\frac{E_{11}}{G_{13}}\right)\right]. \tag{6}$$

It is noteworthy that the crack length (a) should be replaced with the length of the uncracked length (c) in Eqs. 1-4. Based on the analysis, equations, similar to the aforementioned may be derived also for the OLB specimen. The compliance of the OLB specimen becomes [11]:

$$\begin{aligned} C^{OLB} = {} & \frac{s^2c^3}{8bh^3E_{11}L^2}\left[1+8\frac{a}{c}+16\frac{aL}{c^2}+32\frac{aL^2}{c^3}+16\frac{Ls(s-4L)}{c^3}\right]+\frac{s[4L(2L-s)-sc]}{8bhkG_{13}L^2}+ \\ & +\frac{s^2c^3}{8bh^3E_{11}L^2}\left[5.07\left(\frac{h}{c}\right)\left(\frac{E_{11}}{E_{33}}\right)^{\frac{1}{4}}+8.58\left(\frac{h}{c}\right)^2\left(\frac{E_{11}}{E_{33}}\right)^{\frac{1}{2}}+2.08\left(\frac{h}{c}\right)^3\left(\frac{E_{11}}{E_{33}}\right)^{\frac{3}{4}}\right]+ \\ & +\frac{s^2c^3}{8bh^3E_{11}L^2}\left[0.98\left(\frac{h}{c}\right)\left(\frac{E_{11}}{G_{13}}\right)^{\frac{1}{2}}+0.43\left(\frac{h}{c}\right)^2\left(\frac{E_{11}}{G_{13}}\right)\right]+\frac{1}{\pi}\frac{3s^2c^2}{4bh^2E_{11}L^2}\left(\frac{E_{11}}{G_{13}}\right)^{\frac{1}{2}}. \end{aligned} \tag{7}$$

The reduced bending moments for the OLB coupon are: $M_1=P(2L-s)/2L$, $M_2=0$. The application of Eq. 1 results in the following SERR components:

$$\begin{aligned} G_{I}^{OLB} = {} & \frac{12P^2s^2c^2}{16b^2h^3E_{11}L^2}\left[1+0.85\left(\frac{h}{c}\right)\left(\frac{E_{11}}{E_{33}}\right)^{\frac{1}{4}}+0.71\left(\frac{h}{c}\right)^2\left(\frac{E_{11}}{E_{33}}\right)^{\frac{1}{2}}\right. \\ & \left.+0.32\left(\frac{h}{c}\right)\left(\frac{E_{11}}{G_{13}}\right)^{\frac{1}{2}}+0.1\left(\frac{h}{c}\right)^2\left(\frac{E_{11}}{G_{13}}\right)\right], \end{aligned} \tag{8}$$

$$G_{II}^{OLB} = \frac{9P^2s^2c^2}{16b^2h^3E_{11}L^2}\left[1+0.22\left(\frac{h}{c}\right)\left(\frac{E_{11}}{G_{13}}\right)^{\frac{1}{2}}+0.048\left(\frac{h}{c}\right)^2\left(\frac{E_{11}}{G_{13}}\right)\right]. \tag{9}$$

3. EXPERIMENTS AND DATA REDUCTION

The fixtures for the ONF and OLB tests are illustrated in Figure 2. The tests were carried out using an Amsler testing machine under displacement control. The load-deflection data was measured, the latter was monitored by the dial gauge, shown in Figures 2a and b. The full span length was 2L=151 mm, the position of the external load was s=47.5 mm (refer to Figure 1). The contact regions above the supports were slightly roughened in order to prevent the longitudinal sliding.

Two kinds of measurements were carried out. At the first stage initiation tests were performed on both configurations. In the case of the ONF test the specimens with initial crack length from 50 to 105 mm with 5 mm increment were prepared ($0.33\cdot 2L\le a\le 0.69\cdot 2L$). For the OLB test the crack length range from 55 to 115 mm ($0.36\cdot 2L\le a\le 0.76\cdot 2L$) with 5 mm increment was investigated. If the initial crack length was higher than 105 mm in the ONF test and 115 mm in the OLB test, respectively, we were not able to facilitate crack initiation and large displacement of the specimens occurred. The

specimens were tested to failure at the crack length of interest and the critical load and deflection were recorded.

At the second stage propagation tests using six ONF and OLB specimens with a_0=50 mm initial crack length were performed. In this case a millimeter scale was traced on the lateral sides of the specimens, the crack length was measured visually by following the crack front on the upper surface of the specimens and the position of the crack tip was marked. The compliance of the specimens was determined at each crack length.

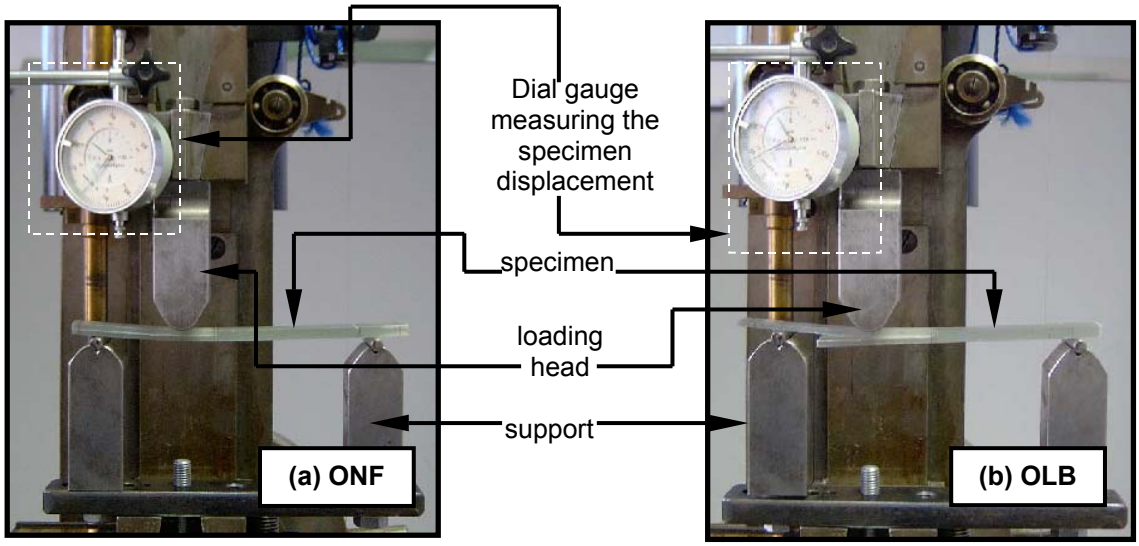

Figure 2 – Over-notched flexure (a) and over-leg bending (b) tests for interlaminar fracture.

3.1 Compliance Calibration

The compliance of the ONF [6] and OLB [11] specimens may be written as

$$C = C_0 + n(a - 2L)^3 . \tag{10}$$

The coefficients, C_{02} and n may be determined by using least square fitting. The SERR may be calculated by using the Irwin-Kies expression:

$$G_C = \frac{P^2}{2b}\frac{dC}{da}. \tag{11}$$

3.2 Direct beam theory

As it will be shown later the compliance calibration gives misleading result in the case of the ONF test if crack initiation is considered. Therefore, the direct beam theory is also applied. In this case the flexural moduli of the specimens is eliminated. The relevant equation based on direct beam theory are:

$$G_{II}^{ONF} = \frac{9P\delta}{2b(2L-a)}\frac{1}{\theta},\ \theta = 1 + \frac{4a}{2L-a} + \frac{8aL}{(2L-a)^2} + \frac{16L^2a}{(2L-a)^3} + \frac{8Ls(s-4L)}{(2L-a)^3}, \tag{12}$$

where P is the load, δ is the experimentally determined specimen displacement, respectively.

4. RESULTS AND DISCUSSION

4.1 Initiation tests

The recorded load/displacement curves are shown in Figure 3. The response was essentially linear elastic in both specimens, which justifies the application of the linear elastic fracture concepts. The range of the applied load is somewhat higher in the case of the ONF test. In spite of this, we may observe that the OLB specimen requires higher displacement values to reach the point of fracture at each crack length.

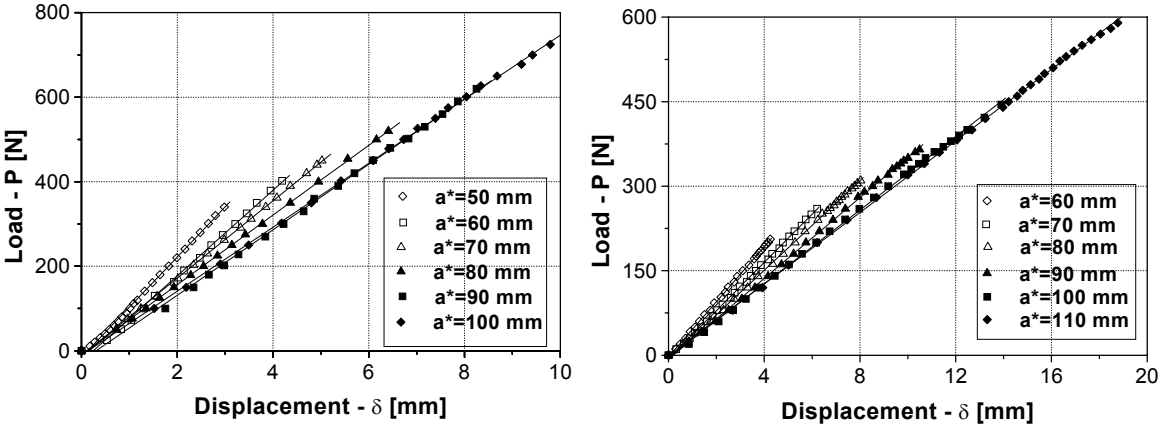

Figure 3 - Load/displacement curves up to fracture initiation, ONF test (a), OLB test (b).

The measured compliance values and the calculated curve are plotted in Figure 4a for the ONF specimens. The beam theory-based solution agrees well with the measured values. In the case of the OLB specimen (Figure 5a) the agreement is again excellent. It should be mentioned that in both configurations the characteristic distance is the length of the uncracked region (c).

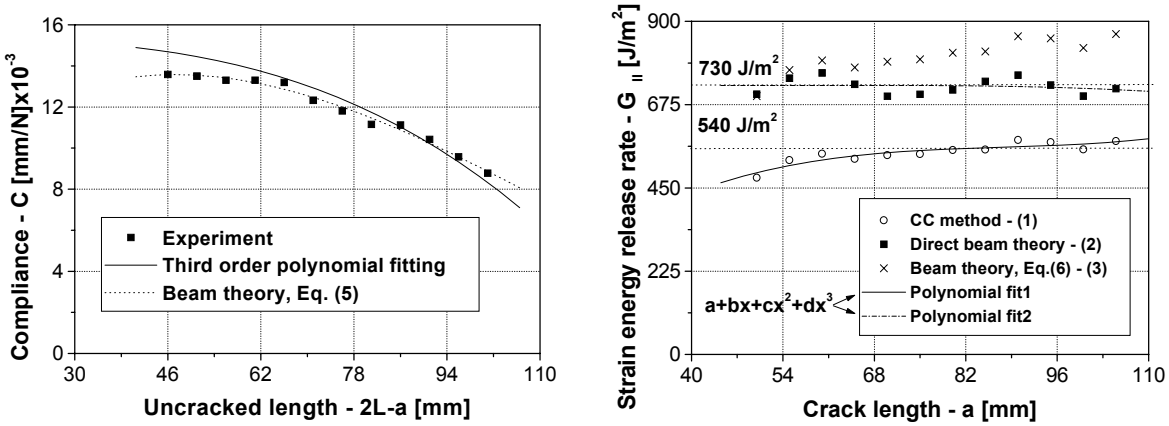

Figure 4 - Measured and calculated compliance from initiation tests (a). SERR against the crack length (b) (ONF specimen).

Three reduction techniques were used to calculate the mode-II SERR by the ONF test. Its values against the crack length are plotted in Figure 4b. It seems that the CC method gives somewhat surprising results. The beam theory and direct beam theory show approximately a 790 and a 730 J/m^2

steady state values, respectively, while the value of 540 J/m^2 was obtained by the CC method. Therefore, the result of the CC method is slightly doubtful and its application is not recommended in this case. The mixed-mode I/II SERR by the OLB test is illustrated in Figure 5b. In this case the correlation between the analytical equations and the CC method is better, however this time the beam theory slightly overpredicts the values by the CC method. Overall, this is not significant. The relevant steady state values are 715 J/m^2 by beam theory and 650 J/m^2 by means of the CC technique.

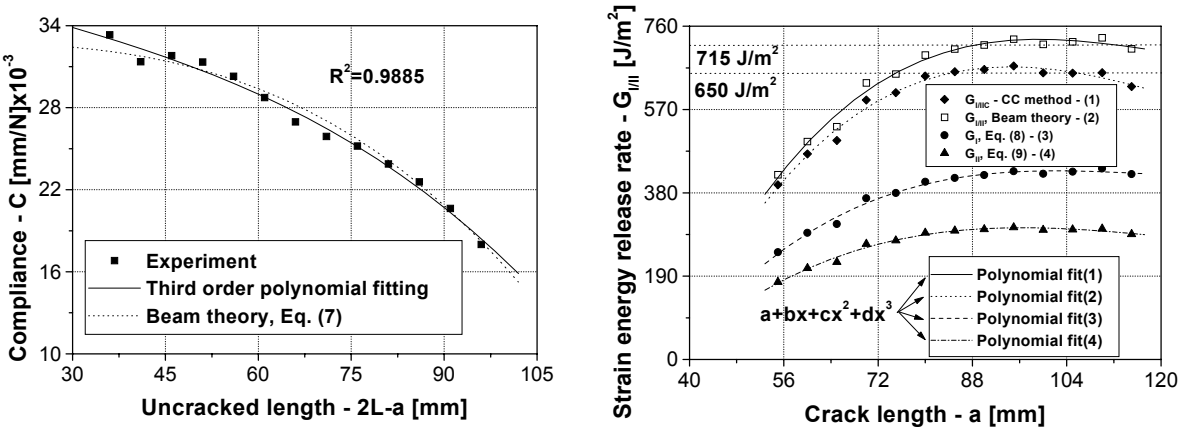

Figure 5 - Measured and calculated compliance from initiation tests (a). SERR against the crack length (b) (OLB specimen).

4.2 Propagation tests

The load-displacement curves are demonstrated in Figure 6. A remarkable feature is that the load-displacement curves exhibit a bilinear character. For the ONF specimen the range of the applied load (Figure 6a) is about two times higher compared to the initiation tests (refer to Figure 3a). On the other

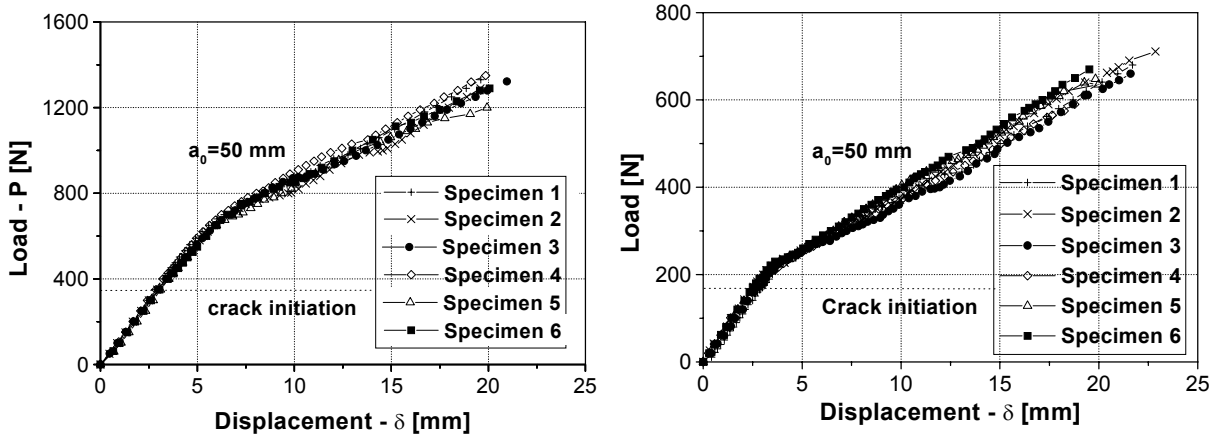

Figure 6 - Load/displacement curves, propagation tests. ONF specimen (a), OLB specimen (b).

hand the range of the applied load is eventually the same in propagation and initiation tests if we investigate the results by the OLB test (refer to Figure 3b and Figure 6b). The stiffness of the system was higher in the ONF setup, this may establish the relatively large load values.

The measured compliance values and the calculated compliance curve are depicted in Figure 7a for the propagation test of one ONF specimen. The experimentally measured compliance values

correspond well with the analytical curve. For the OLB configuration (Figure 7c) essentially the same compliance curves were determined under crack propagation as it was shown in Figure 5a.

The propagation SERR is plotted in Figures 7b and d. Focusing our attention to Figure 7b we may observe that the mode-II toughness reaches a clear plateau value, its average value based on six specimens which is 2787 J/m^2 as determined by the CC method. The result of the beam theory

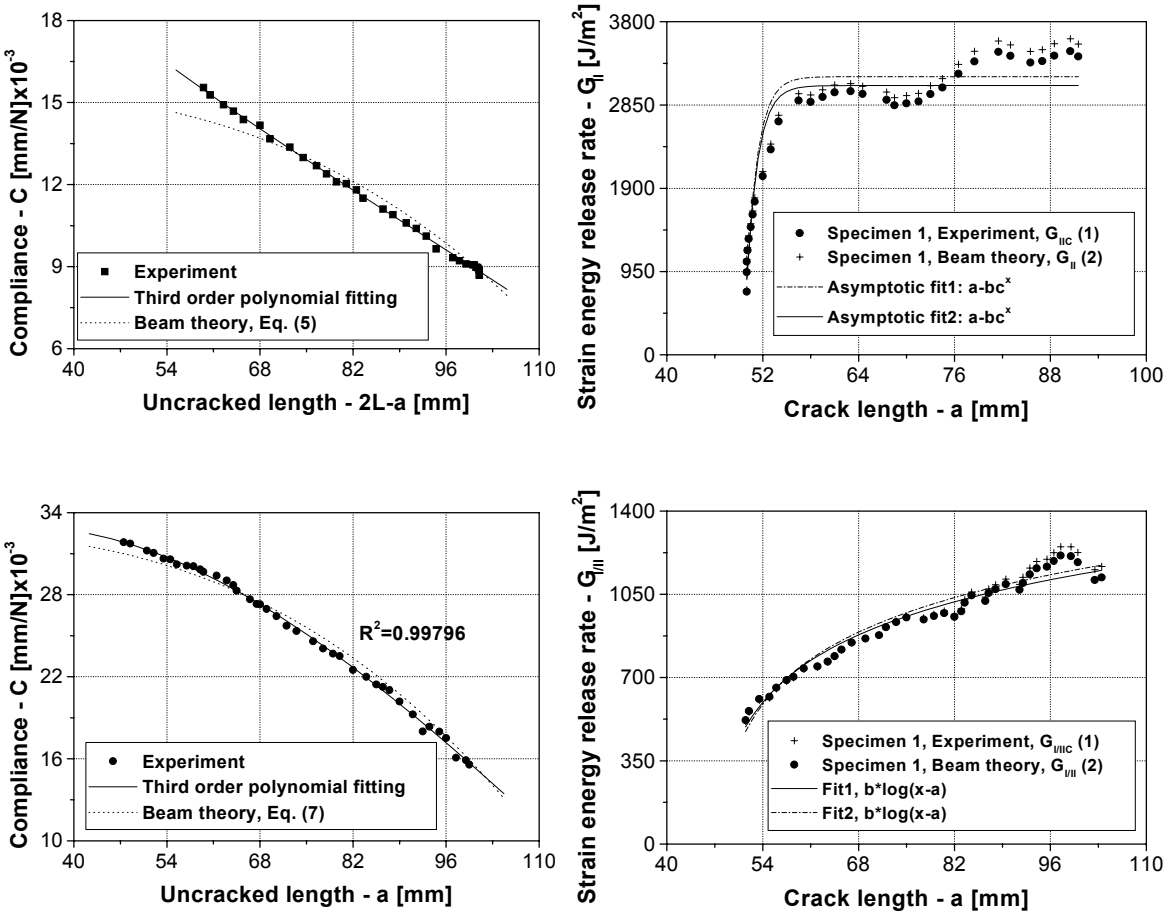

Figure 7 - Measured and calculated compliance from the propagation test of one ONF (a) and OLB (c) specimen. G_{II}-a data from ONF test (b). $G_{I/II}$-a data from OLB test (d).

(2817) closely agrees with the results by CC method. The same conclusions may be established if we consider the results by the OLB test (Figure 7d). However, in the latter case there is not a clear plateau value, which may be explained by the fact that the OLB specimen is mode-I dominated. Overall, the strain energy release rate grows up to 1250 J/m^2.

Davies et al. [7] presented mode-II critical strain energy release rates within 1500-2000 J/m^2 for glass/epoxy composite using the mode-II ELS coupon. The significance of the employed data reduction is highlighted in this work. For mixed-mode the single leg four-point bend (SLFPB) specimen seems to be a reasonable alternative for comparison. Tracy et al. [15] reported 1500 and 1750 J/m^2 plateau values for carbon epoxy systems. Although the steady-state values are different compared to our results, all these authors have found the same trends as it was shown in Figures 4b, 5b, 7b and 7d.

6. CONCLUSIONS

The interlaminar fracture in unidirectional glass/polyester composite was investigated by using the mode-II ONF and the mixed-mode I/II OLB specimens. The experimental data was evaluated by using linear beam theory, the compliance calibration method and the direct beam theory. The initiation SERR was found to reach a plateau value in both configurations. The crack propagation tests revealed that the mode-II toughness by ONF test also reach a clear steady state value. In contrast the mixed-mode toughness proved the so-called R-curve behavior. Overall, a very good agreement was found between the analytical and experimental reduction techniques. The ONF and OLB specimens were found to be efficient tools to examine the fracture properties of the used composite material.

7. REFERENCES

[1] Schön J, Nyman T, Blom A, Ansell H. A numerical and experimental investigation of delamination behaviour in the DCB specimen. *Composite Science and Technology* 2000;60:173-184.

[2] Carlsson LA, Gillespie J W, Pipes RB. On the analysis and design of the end notched flexure (ENF) specimen for mode II testing. *Journal of Composite Materials* 1986;20:594-604

[3] Davies P, Ducept F, Brunner AJ, Blackman BRK, de Morais AB. Development of a standard mode II shear fracture test procedure. *Proceedings of the 7th European Comference on Composite Materials* (ECCM-7) Vol. 2, pp 9-15, London, May 1996.

[4] Wang H, Vu-Khanh T. Use of end-loaded-split (ELS) test to study stable fracture behaviour of composites under mode-II loading. *Composite Structures* 1996;36:71-79

[5] Davies P, Casari P, Carlsson LA. Influence of fiber volume fraction on the interlaminar fracture toughness of glass/epoxy using the 4ENF specimen. *Composites Science and Technology* 2005;65:295-300.

[6] Wang W-X,Takao Y, Nakata M. Effects of friction on the measurement of the mode II interlaminar fracture toughness of composite laminates. *Proceedings of the 14th International Conference on Composite Materials*, San Diego, California, USA, July 14-18, 2003.

[7] Qiao P, Wang J, Davalos JF. Analysis of tapered ENF specimen and characterization of bonded interface fracture under mode-II loading. *International Journal of Solids and Structures* 2003;40:1865-1884.

[8] Reeder JR., Crews JR. Mixed-mode bending method for delamination testing. *AIAA Journal* 1990;28:1270-1276.

[9] Davidson BD, Sundararaman V. A single leg bending test for interfacial fracture toughness determination. *International Journal of Fracture* 1996;78:193-210.

[10] Hashemi S, Kinloch J, Williams JG. The effects of geometry, rate and temperature on mode I, mode II and mixed-mode I/II interlaminar fracture toughness of carbon-fibre/poly(ether-ether ketone) composites. *Journal of Composite Materials* 1990;24:918-956.

[11] Szekrényes A, Uj J. Modified single-leg bending test for mixed-mode I/II interlaminar fracture in composites. *21st Danubia-Adria Symposium on Experimental Methods in Solid Mechanics*, september 29-october 2, 2004, Brijuni/Pula, Croatia.

[12] Szekrényes A, Uj J. Comparison of some improved solutions for mixed-mode composite delamination coupons. *Composite Structures* 2005 (to appear).

[13] Wang J, Qiao P. Novel beam analysis of the end notched flexure specimen for mode-II fracture. *Engineering Fracture Mechanics* 2004;71:219-231.

[14] Szekrényes A, Uj J. Mode-II fracture analysis in unidirectional E-glass/polyester composite. *Journal of Composite Materials* 2005 (to appear).

[15] Tracy GD, Feraboli P, Kedward KT. A new mixed mode test for carbon/epoxy composite systems. *Composites Part A: Applied Science and Manufacturing* 2003;34:1125-1131.